Journal of Nuclear Medicine, published on September 3, 2019 as doi:10.2967/jnumed.119.232603

Non invasive PET imaging of CDK4/6 activation in Breast Cancer

Nicholas Ramos,[1] Jairo Baquero-Buitrago,[1] Zakia Ben Youss Gironda,[1] Youssef Zaim Wadghiri,[1] Thomas Reiner,[2,3,4] Fernando E. Boada,[1] Giuseppe Carlucci[1]*

[1] Center for Advanced Imaging Innovation and Research (CAI^{2}R), NYU School of Medicine, New York, NY, USA; Center for Biomedical Imaging, Dept. of Radiology, NYU School of Medicine, New York, NY, USA

[2] Department of Radiology, Weill Cornell Medical College, New York City, NY 10065, United States;

[3] Department of Radiology, Memorial Sloan Kettering Cancer Center, New York City, NY 10065, United States;

[4] Chemical Biology Program, Memorial Sloan Kettering Cancer Center, New York City, NY 10065, United States;

*Corresponding author: G. Carlucci, PhD.

https://orcid.org/0000-0001-7494-335X

Department of Radiology, NYU School of Medicine, New York, NY, 10016, USA

Email: giuseppe.carlucci@nyulangone.org

Abstract

The cell cycle is a progression of four distinct phases (G1, S, G2, M), with various cycle proteins being essential in regulating this process. We aimed to develop a radiolabeled Cyclin Dependent Kinase 4/6 (CDK4/6) inhibitor for breast cancer imaging. Our transfluorinated analog (^{18}F-CDKi) was evaluated and validated as a novel PET imaging agent to quantify CDK4/6 expression in ER-positive HER2-negative breast cancer.

Methods: ^{18}F-CDKi was synthesized and assayed against CDK4/6 kinases. ^{18}F-CDKi was prepared with a 2-step automated synthetic strategy that yielded the final product with remarkable purity and molar activity. In vitro/in vivo biologic specificity was assessed in a MCF-7 cell line and in mice bearing MCF-7 breast tumors. Non radioactive Palbociclib (Inbrance, Pfizer®) was used as blocking agent to investigate the binding specificity and selectivity of ^{18}F-CDKi.

Results: ^{18}F-CDKi was obtained with an overall radiochemical uncorrected yield of 15% and radiochemical purity > 98 %. The total synthesis time from the start of synthesis to final injectable formulated tracer is 70 minutes. The retention time reported for ^{18}F-CDKi and ^{19}F-CDKi is 27.4 min as demonstrated by co-injection with ^{19}F-CDKi in a HPLC. *In vivo* blood half-life [$t_{1/2}$(weighted) = 7.03 minutes], and octanol/water phase partition coefficient ($logD_{O/W}$ = 1.91 ± 0.24) showed a mainly lipophilic behavior. ^{18}F-CDKi is stable in vitro and in vivo (>98% at 4h post injection) and maintained its potent targeting affinity to CDK4/6. Cellular uptake experiments performed in the MCF-7 breast cancer cell line (ER-positive/HER_2-negative) demonstrated specific uptake with a maximum intracellular concentration of ~65% as early as 10 minutes post incubation. The tracer uptake was reduced to <5% when cells were co-incubated with a molar excess of Palbociclib. In vivo imaging and ex-vivo biodistribution of ER-positive/HER-2 negative MCF-7 breast cancer models showed a ~4%ID/g tumor specific uptake (reduced to ~0.3%ID/g with a 50-fold excess of cold palbociclib). A comprehensive biodistribution analysis also revealed a significantly lower activation of CDK4/6 in non-targeting organs.

Conclusion: ^{18}F-CDKi represents the first ^{18}F positron emission tomography (PET) CDK4/6 imaging agent and a promising imaging agent for ER-positive HER2-negative breast cancer.

Running Title: CDK4/6 radio inhibitor for PET imaging

Keywords: Cell Cycle, CDK4/6, PET/CT imaging, Breast Cancer, MCF-7

INTRODUCTION

The cell cycle is a progression of four distinct phases (G1, S, G2, M) that cells use to maintain the integrity of their genomes (*1-5*). Sophisticated cell cycle pathways and cell cycle arrest proteins are used to remediate DNA damage, to efficiently control the cell cycle and DNA replication (*5,6*), and to trigger DNA repair. Alterations in the cell cycle and uncontrolled proliferation are well known hallmarks of cancer (*7,8*). Cyclin Dependent Kinases 4/6 (CDK4/6) are two apical kinases that control the cell cycle by arresting the progression in case of DNA damage (*9-12*). Subsequently to cell damage, cycD1-CDK4/6 complex arrests the cell cycle progression in G1 to limit the proliferation of the DNA-damaged cells (*13*). The dysregulation of the cycD1-CDK4/6 axis appears to be an early step in cancer pathogenesis and cycD1 overexpression is shown as early as ductal carcinoma in both, in situ and in metastatic lesions (*7,13-17*). Notably, amplification of genes encoding D-type cyclins is commonly observed in human cancer, and correlates with increased levels of cyclin D protein. A major target of CDK4 and CDK6 during cell-cycle progression is the retinoblastoma protein (Rb). CDK4/6-cycD1 complexes phosphorylate Rb. When Rb is phosphorylated, it dissociates from the E2F family that enable cell cycle progression to the S phase. Selective inhibitors act on CDK4/6 kinases, dephosphorylate Rb and stall the cell-cycle progression in G1. This action inhibits the proliferation of cancer cells and triggers the DNA-damage repair. Hence, it is intuitive that efficient inhibition of CDK4/6 can enhance and amplify the chemotherapeutic effects of therapies aimed at targeting the cell cycle proliferation, checkpoints and arrest.

Amplification of CDK4/6 and cycD1 has been reported in a significant number of cancers and the overexpression of cycD1 was observed in >60% of all breast cancers (*14,18-20*). Furthermore, amplification and overexpression of cycD1 and CKD4/6 has been described in patients with head and neck cancer (*21*), non-small-cell lung cancer (*22*), melanoma (*23-25*) and glioblastoma (*26*). Gene amplification of cycD1 was found to be most frequent in luminal A, B and HER2 enriched breast cancer subtypes (frequencies of alteration: 29%, 58%, and 38%, respectively) (*7*). Similarly, amplifications of CDK4/6 were more common in the luminal A, B and human epidermal growth factor receptor 2 (HER_2) enriched subgroups (14%, 25%, and 24%, respectively) (*7*). Moreover, in patients with luminal estrogen receptor (ER)-positive breast cancer, which represents approximately 75% of all breast cancers, cycD1-CDK4/6 is expressed at a high-level (*15*). Thus, ER+, luminal breast cancer is the typical and the most indicated model for

investigating the effectiveness of CDK4/6 inhibitors and served as a platform for our initial biological evaluation (*7*).

We developed ^{18}F-CDKi, a PET radiolabeled version of Palbociclib (Inbrance®, Pfizer) to image non-invasively kinase expression in breast cancer models. Specifically, we introduced an F-18 prosthetic group (^{18}F-fluorobenzoic acid, ^{18}F-FBA), on the terminal piperazine (*27*) and synthesized a novel PET active functional molecule. We aimed to determine if i) ^{18}F-CDKi has suitable pharmacokinetic properties for non-invasive PET imaging and ii) whether the tracer is selective for CDK4/6. For both in vitro as well as in vivo evaluation, a breast cancer ER-positive HER2-negative cell line (MCF-7) was used.

To our knowledge, this is first in class radiolabeled inhibitor able to target specifically CDK4/6. Because of these promising results in mouse models, we anticipate ^{18}F-CDKi to have a high prognostic value for tumor imaging and treatment response monitoring.

MATERIALS AND METHODS

Materials

No carrier added ^{18}F-fluoride was produced by the (p,n) reaction of [^{18}O]H_2O in an RDS-112 cyclotron (Siemens; Knoxville, TN). Potassium carbonate, kryptofix, ethyl 4-nitrobenzoate, *N,N,N′,N′*-Tetramethyl-*O*-(1*H*-benzotriazol-1-yl)uronium hexafluorophosphate (HBTU), triethlyamine, ammonium formate, sodium hydroxide, hydrochloric acid, acetonitrile and dimethyl sulfoxide were purchased from Millipore-Sigma (Milwaukee, WI, USA) and used without further purification unless otherwise stated. Palbociclib hydrochloride was purchased from Selleck (Houston, TX). ATP was obtained from PerkinElmer (Boston, MA). Ethanol was purchased from Thermo Fisher (Waltham, MA). Sep-Pak Accell Plus QMA and C18 sep-pak cartridges were purchased from Waters (Milford, MA). Semi-preparative high-pressure liquid chromatography (HPLC) was conducted in the GE TRACERlab™ FX2N under the following HPLC conditions: Phenomenex Gemini C6 phenyl column, 10x250 mm, 10 um; mobile phase: 64% 75 mM AMF and 36% MeCN; 5 mL/min (Method A). Analytical HPLC was performed using a Shimadzu binary LC-20AR HPLC gradient pump with an inline SPD-20A variable wavelength UV/VIS detector, and a flow count unit with a PMT detector using a Phenomenex C6 Gemini reverse-phase column, 4.6x250 mm 5 µm with a mobile phase of 64% 75 mM AMF and 36% MeCN; 2 mL/min (Method B). Analytical chromatograms were collected by an analog-to-digital converter using Lab

Solutions software. Preparative and analytical HPLC analyses of ^{18}F-labeled compounds were calibrated with the corresponding ^{19}F analogues. Radioactivity in blood half-life, cell uptake and biodistribution studies was quantified with a WIZARD^2 automatic γ-counter (PerkinElmer, Boston, MA). Radioactivity in blood half-life, cell uptake and biodistribution studies was quantified with Inveon PET/CT (Siemens Medical Solutions, Knoxville, TN) and reconstructed using Inveon Research (Siemens Medical Solutions, Knoxville, TX). All F-18 and F-19 CDKi final products were formulated in 10% Ethanol/ 90% Saline 0.9%.

Cell Culture

Phosphate buffered saline (PBS) and Dulbecco's Modified Eagle Medium (DMEM) were purchased from Thermo Fisher (Waltham, MA). MCF-7, a human ER-positive, HER2-negative breast cancer cell line was purchased from ATCC (Manassas, VA). DMEM contained 10% (vol/vol) heat inactivated fetal bovine serum, 100 IU penicillin, and 100 μg/mL streptomycin.

Mouse Model

Female athymic nude CrTac:NCr-Foxn1nu mice (n=35) were purchased from Taconic Laboratories (Hudson, NY). 20 mice received subcutaneous injections with 2x10^6 human MCF-7 cancer cells in Matrigel® (BD Biosciences, San Jose, CA) into each right shoulder and were allowed to grow for approximately two months until the tumors reached ~10 mm in diameter. All mice were supplemented with 60 days 0.72 mg slow release estradiol pellets purchased from Innovative Research of America (IRA, Sarasota, FL) implanted in the left flank. Mice were anesthetized (isoflurane 1.5%, 2 L/min medical air) during tumor implantation and microPET imaging.

15 mice were used for blood half-life measurements and in vivo stability studies. All animal experiments were conducted in accordance with protocols approved by the Institutional Animal Care and Use Committee of NYU Langone Health and followed NIH guidelines for animal welfare.

Preparation of ^{19}F-CDKi

To a solution of palbociclib in DMSO (20 mg, 0.04 mmol), fluorobenzoic acid (15 mg, 0.1 mmol), HBTU (45 mg, 0.1 mmol) and triethylamine (12 mg, 0.1 mmol) were added and the solution reacted at 37°C for 24 hours. The resulting solution was filtered and purified by reverse phase HPLC to the desired derivative (yield = 70%), dried and lyophilized to yield the final

product. Electrospray ionization mass spectrometry (ESI-MS) spectra were recorded with a Shimadzu LC-2020 with electrospray ionization SQ detector.

Radiochemistry

No-carrier-added (n.c.a.)^{18}F-fluoride was obtained via the ^{18}O(p,n)^{18}F nuclear reaction of 11-MeV protons in a RDS Eclypse (Siemens Medical Solutions, Knoxville, TN). Synthesis was automated using a FX2N module (GE Healthcare, Chicago, IL). Briefly, a QMA cartridge containing cyclotron-produced ^{18}F fluoride ion was eluted with a solution containing 9 mg Kryptofix [2.2.2] (4,7,13,16,21,24-hexaoxa-1,10-diazabicyclo[8.8.8]hexacosane), 0.08 mL 0.15 M K_2CO_3 and 1.92 mL MeCN into a 5 mL reaction vial. Water was removed azeotropically at 120 °C. 1 mg of ethyl 4-nitrobenzoate was dissolved in 300 µL of DMSO and added to the reaction vial, heated to 150 °C for 15 minutes and then cooled to room temperature. Following, 150 µL of 1M NaOH was added. The reaction mixture was stirred for 1 min and 150 µL of 1M HCl was added to quench. Then, 2 mg of Palbociclib dissolved in 200 µL of DMSO was added followed by 10 mg of HBTU dissolved in 200 µL of DMSO and 30 µL of Et_3N. 400 µL MeCN followed by 700 µL H_2O was then added and the solution was injected onto a C6-Phenyl analytical HPLC column and eluted under isocratic conditions. Then, the collected fraction was passed through a C18 light-SepPak® cartridge and ^{18}F-CDKi was eluted using EtOH (400 µL). The solution was then diluted with 0.9% saline to 10% EtOH. Molar activity was determined by dividing the activity present in the final formulated product (GBq) by the material remaining in the formulated product after purification (moles) and was determined using a UV calibration curve (λ = 254 nm).

Chemical Hydrophobicity Index and Octanol/Water partition coefficient

The Chemical Hydrophobicity Indices (CHI) were measured using a previously developed procedure (*28,29*). Briefly, reverse phase HPLC was used to measure the retention times of a set of standards with known CHI. A standard curve was then created to calculate the CHI of ^{19}F-CDKi based on the HPLC retention time. The lipophilicity of the ^{18}F-CDKi was acquired by adding 0.09 mBq to a mixture of 0.5 mL of 1-octanol and 0.5 mL of 25 mM phosphate buffered saline (pH 7.4) and mixed for 5 minutes. Then, the mixture was centrifuged at 15.000 rpm for 5 minutes. 100 µL samples were obtained from organic and aqueous layers, and the radioactivity of the samples were measured in a WIZARD^2 automatic γ-counter. The experiment was performed in triplicate, and the resulting $logP_{ow}$ was calculated as the mean ± SD.

Blood Half-Life

The blood half-life of ^{18}F-CDKi was calculated by measuring the activity of blood samples collected at different time points p.i. (5, 15, 30, 45, 60, 90 and 120 minutes). Female nude mice (n = 3) were injected via lateral tail vein with ^{18}F-CDKi (and blood samples obtained by retro-orbital bleed using tared capillary tubes. Samples were weighed, and activity was measured by γ-counter. The blood half-life was calculated using Graph Prism 7 (GraphPad Software, La Jolla, CA) using a two-phase decay least squares fitting method and expressed as %ID/g.

In Vivo/Ex Vivo Blood Stability

^{18}F-CDKi (7.4 mBq) was injected in healthy athymic nude mice (n=15) via tail injection. Mice were sacrificed at different time points (0, 60, 120, 180, 240 min p.i.) and blood was collected. 750 μL of MeCN were added to the collected blood, then centrifuged (5 minutes at 5000 rpm) to pellet blood cells and proteins. The supernatant was collected, diluted with 750 μL of H_2O and injected onto a HPLC. The blood stability was measured by HPLC analysis (Method B).

IC50 Binding Affinity and Competitive Inhibitory Displacement

IC_{50} values were determined using a competitive ATP quantitative assay as reported elsewhere (*30*) and ^{19}F-CDKi. MCF-7 cells were cultured at 37°C for 4 h. Then, ^{19}F-CDKi or vehicle was added at different concentration and incubated at 37 °C for 96 h. Cell viability was then assessed using CellTiter-Glo® Luminescent Assay (Promega, Madison, WI), used accordingly to manufacturer's guidelines. Cell viability inhibition (%) was calculated according to the formula [1 - (mean luminosity of treated sample/mean luminosity of vehicle control)] x 100. IC_{50} for growth or viability inhibition was calculated using Graph Prism 8 (GraphPad Software Inc, La Jolla, CA). We also used ^{18}F-CDKi and palbobiclib for competitive displacement studies. MCF-7 cells were seeded in a 12 wells plate ($1x10^5$ cells 24 h prior the experiment). The next day, a fixed concentration of ^{18}F-CDKi (50 nM) was co-incubated with linearly doubling concentrations of palbociclib (from 0 to 500 nM) at 37 °C for 2 h. Then, the cells were washed twice with PBS, lysed with 1N NaOH, and the activity (CPM) measured in a γ-counter for bound ^{18}F radioligand. The percentage of bound radioligand was finally plotted against palbociclib concentration. Competitive displacement curves were fitted using Graph Prism 8 (GraphPad Software Inc, La Jolla, CA).

In Vitro Uptake

MCF-7 cells were seeded in a 6 well plates ($5x10^6$ cells 24 hours prior the experiment). The next day, ^{18}F-CDKi was added alone or together with a 50-fold excess Palbociclib and incubated at 37 ºC for 1 h. After 1 h, cells were firstly washed three times with PBS, then lysed with 1N NaOH, and finally media and cells counted in a γ-counter. The percentage of bound/unbound radioligand at each time point was measured in triplicate and plotted as a function of time.

MicroPET/CT Imaging

Twelve subcutaneous MCF-7 implanted athymic nude mice were divided in two groups (blocked and^{18}F-CDKi) and administered with ^{18}F-CDKi (~7.4 mBq) via tail vein injection. Approximately 5 min prior to PET acquisition, mice were anesthetized by inhalation of a mixture of isoflurane (Baxter Healthcare, Deerfield, IL, USA; 2% isoflurane, 2 L/min medical air) and positioned in the scanner. Anesthesia was maintained using a 1% isoflurane/O_2 mixture. PET data for each mouse was recorded and acquired at 30 min p.i and at 120 min p.i. Blocking studies were performed after a pre-injection of 50-fold excess palbociclib (8.4 nmol, 3.8 μg, 30 min before). The duration of the microPET/CT imaging sessions was 20 min each.

Biodistribution

Biodistribution of ^{18}F-CDKi was performed in subcutaneous MCF-7 bearing athymic nude mice (n = 8). Mice were divided (n= 4/group) in blocked and unblocked (50-fold excess palbociclib, 2 nmol, 0.95 μg, 30 minutes before) and administered with ^{18}F-CDKi via tail vein injection (1.85 mBq). At 120 minutes post injection of the radioligand, the mice were sacrificed and organs of interest were collected. Organs were weighed, and activity was measured with a WIZARD^2 automatic γ-counter (PerkinElmer, Boston, MA). The radiopharmaceutical uptake was expressed as a percentage of injected dose per gram (%ID/g) using the following formula: [(activity in the target organ/grams of tissue)/injected dose]x100%.

Statistical Analysis

All data are expressed as mean ± SD. Differences between mouse cohorts were analyzed with the 2-tailed unpaired Student's t-test and were considered statistically significant when $P < 0.05$.

RESULTS

Chemistry and Radiochemistry

^{18}F-CDKi was synthesized by a 2-steps method (Fig. 1A and Supplemental Fig. 1). The final F-18 transfluorinated product (Fig. 1B) was obtained with an overall uncorrected yield of ~15% (n = 4) and a radiochemical purity > 98%. Molar activity was 44 GBq/μmol and the total automated synthesis time is 80-90 minutes. The retention time reported for ^{18}F-CDKi and [^{19}F]-CDKi is ~17 min as demonstrated by co-injection with ^{19}F-CDKi in a HPLC (Fig. 1C). ^{19}F-CDKi (Fig. 2A, final yield ~ 80%) was obtained with high purity as shown by LC-MS. Observed m/z for ^{19}F-CDKi was 566 ([M]+H) and 564 ([M]-H) in positive and negative polarity mode (expected m/z for ^{19}F-CDKi = 565) (Supplemental Fig. 2B). No unreacted palbociclib (mw = 447.5 g/mol) was observed after purification indicating a high chemical purity of the HPLC purified ^{19}F-CDKi.

Cellular Binding Specificity and Cell Internalization

^{18}F-CDKi maintained a potent targeting affinity to CDK4/6 (~13nM) (Fig. 2A). The competitive displacement of palbociclib in MCF-7 cells was an indication of the similar inhibition effect of ^{18}F-CDKi to ^{19}F-CDKi (~18 nM) in MCF-7 cells (Supplemental Fig. 3). Cell-associated uptake of ^{18}F-CDKi is shown in Supplemental Fig. 4. Cell uptake could be blocked nearly completely (>98%) by addition of an excess of cold, unlabeled palbociclib ($P < 0.0001$) suggesting the high cellular specificity of ^{18}F-CDKi. Cellular uptake experiments performed in MCF-7 breast cancer cell line (ER-positive/HER_2-negative) demonstrated a maximum intracellular concentration of ~65% at already 10 minutes post incubation, when the internalization rate reached a plateau.

Stability and Pharmacokinetics

The *in vivo* blood half-life [$t_{1/2}$(weighted)] was 7.03 minutes (Fig. 2B). ^{18}F-CDKi was stable in both in vitro and in vivo with more than 98% of the parent compound intact after 4 h of incubation (>98% at 4h post injection). Octanol/water phase partition coefficient ($logD_{O/W}$) is 1.91 ± 0.24 and CHI value is 61.23 (Fig. 2C-E).

In vivo imaging and ex-vivo biodistribution

PET imaging showed a significant specific uptake in the tumor lesion (Fig. 3). MCF-7 xenografts showed a ~ 4%ID/g when mice were injected with ^{18}F-CDKi. Tracer uptake in the tumor decrease to ~0.3%ID/g when mice were blocked with a 50-fold excess of palbociclib. PET imaging and biodistribution data showed that ^{18}F-CDKi is cleared via the hepatobiliary route (Fig.

3 and 4A). High concentration of ^{18}F-CDKi were found in the kidney (7.99 ± 0.7 or 9.6 ± 0.98 %ID/g), liver (6 ± 0.5 or 6.77 ± 1.15 %ID/g) and small intestines (9.6 ± 2.7 or 10 ± 1.19 %ID/g) with relatively low distribution in other tissues (Fig. 4A) at 2 h post injection. A statistical significance in uptake was obtained in the tumor (Fig. 4B). A comprehensive biodistribution analysis revealed also a remarkable tumor-to-blood (>5), tumor-to-muscle (>15) and tumor-to-bone (>10) ratio (Fig. 4C). A complete dataset showing a favorable in vivo PK profile of ^{18}F-CDKi is available in the Supplemental information (Supplemental Fig. 5).

DISCUSSION

In this study, we report on a first in vivo CDK4/6 imaging agent with strong similarities to Palbociclib, the first clinically FDA approved CDK4/6 inhibitor (*31*).

CDK4/6 inhibitors are being intensively studied and several clinical trials were established to study the effects of various compounds in synthetic lethal combination settings (*14,32,33*). A common characteristic to those treatments is the development of resistance (*32,34,35*). Poor oral availability, clearance and metabolism, feedback from other cyclins, lack of target enzyme are all hypotheses for the innate and the development of acquired resistance to CDK4/6 inhibitors (*34*). However, none of the potential resistance mechanisms demonstrated in preclinical settings could be further confirmed in clinical studies (*32-34*). For this reason, we synthesized a radioligand that can reveal whether the drug accumulation in the tumor is limiting the therapeutic efficiency. ^{18}F-CDKi might help to select patient responders or non-responders to CDK4/6 inhibitors. ^{18}F-CDKi might assess whether CDK or palbociclib treatment combinations are well tolerated, even without an increase of febrile neutropenia which is significantly more common in the palbociclib-containing combinations compared to hormonal therapy alone. Moreover, ^{18}F-CDKi can indicate whether treatments necessitate dose interruptions and reductions. Finally, ^{18}F-CDKi may allow to study pharmacodynamic effects of lower doses of palbociclib. This might help to tailor a specific line of treatment in ER-positive HER2-negative breast cancer patients.

Structurally, the introduction of an ^{18}F prosthetic synthon to the piperazine group appeared to be a viable approach for generating a labeled CDK4/6 inhibitor. Firstly, we synthesized and profiled ^{19}F-CDKi, the cold fluorinated analogue of the radiolabeled counterpart. ^{19}F-CDKi was key to assess if the fluorobenzoic tag would impact the compound's biological activity. ^{18}F-CDKi was readily synthesized using a modified published synthetic approached (*36,37*). Minor

modifications for automation purposes were included as well. Synthesis started from conversion of 4-ethyl-nitrobenzoate to 4-^{18}F-fluorobenzoic acid. Subsequent reaction with palbociclib was rapidly accomplished in basic conditions to yield the final ^{18}F-CDKi imaging agent. Following scale-up synthesis and characterization of the radiotracer, we next tested the radiolabeled tracer ^{18}F-CDKi both *in vitro* and *in vivo*. In light of the relevance of palbocilib in treating ER-positive HER2-negative breast cancer, we chose MCF-7 as a mouse model for our *in vitro*/*in vivo* studies.

Initially, we determined the *in vivo* blood half-life and *plasma* stability of ^{18}F-CDKi**.** The tracer displayed a specific intracellular uptake in MCF-7 cells and an IC_{50} in the nanomolar range similar to the parent compound palbociclib (*27*). The insertion of an ^{18}F prosthetic group did not modify the binding properties of CDKi. Furthermore, as for other CDK4/6 inhibitors, our molecule is also an ATP-competitive ligand of CDK4 and CDK6. Herein, as previously reported elsewhere, the IC_{50} is reported with single digit nanomolar potency against both CDK4 and CDK6 kinases (*38*). The blood half-life, following a single bolus intravenous injection, showed a biphasic pharmacokinetic profile with rapid elimination of ^{18}F-CDKi during the first 10 min similar to other small molecule inhibitors (*37,39*). ^{18}F-CDKi shows a marked lipophilic behavior and more than 98% of the tracer was stable in vivo at 4 h p.i.. In subcutaneous MCF-7 xenografts, ^{18}F-CDKi was rapidly washed out from non-target organs resulting in a remarkable tumor-to-non-target tissue at 2 h post-injection. Consistent with CDKi activation and cycD1 overexpression in breast tumors, ^{18}F-CDKi was observed to specifically accumulate in the tumor as proven by the blocking experiment. MCF-7 bearing mice that received an injection of palbocilib prior to the radiotracer showed negligible ^{18}F-CDKi tumor uptake. There is significant promise that more clinical positive outcomes will emerge through a detailed understanding of the biology of CDK4/6 inhibitors (*14,15,33*).

This novel tracer might further be used as a tool to improve patients outcome or design a more personalized combination strategies (*32,34*).

CONCLUSION

^{18}F-CDKi combines high stability, fast penetration, high contrast and rapid washout properties with a remarkable in vitro and in vivo binding to CDK4/6. These results suggest that this probe could offer an early prognostic assessment of treatment response or acquired resistance to CDK4/6 inhibitors. Moreover, with a hybrid imaging technique, such PET ^{18}F-CDKi in

combination with MRI, clinicians might have an alternative approach to tailor precise medical treatments and therapies based on patient CDK4/6 biomarker expression.

DISCLOSURE

No potential conflict of interest relevant to this article exist.

ACKNOWLEDGMENTS

The authors thank the Education and Research Foundation for Nuclear Medicine and Molecular Imaging (2017 ERF-SNMMI for G.C.) for their generous support. This work was supported by National Institutes of Health grants P41 EB017183 (F.B. and G.C.) and R01 CA204441 and P30 CA008748 (for T.R.). The authors thank the Tow Foundation and MSK's Center for Molecular Imaging & Nanotechnology and Imaging and Radiation Sciences Program.

KEY POINTS

QUESTION: Can ^{18}F-CDKi provide an exact and accurate assessment of functional CDK4/6 expression in breast cancer development and progression and can be used to monitor CDK4/6 based treatment?

PERTINENT FINDINGS: The first *in vitro* experiment aiming to analyze pharmacokinetics (PK) and *in vitro* activity revealed that ^{18}F-CDKi (based on Palbociclib, an FDA approved drug) can be a successful PET agent with nearly ideal imaging characteristics. We demonstrated that ^{18}F-CDKi is stable in vitro and in vivo and maintained a potent targeting affinity to CDK4/6. Cellular uptake experiments performed in a MCF-7 breast cancer cell line (ER-positive/HER$_2$-negative) demonstrated specific uptake. Similar significant uptake values were also observed in MCF-7 bearing mouse models. The strong activation of CDK4/6 in cancer cells in concert with its low activation in untransformed healthy cells (as resulted from our tumor-to-non-target tissue ratio calculations) makes ^{18}F-CDKi an ideal imaging agent, first in its class, for CDK4/6 assessment.

IMPLICATIONS FOR PATIENT CARE: ^{18}F-CDKi can improve screening for breast cancer and selection of responders to CDK4/6 therapy. ^{18}F-CDKi allows to quantify CDK4/6 activation (at a cellular level) and to assess CDK4/6 protein status in current translational cancer research.

REFERENCES

1. Jackson SP, Helleday T. Drugging DNA repair. *Science.* 2016;352:1178-1179.

2. Da-Rè C, Halazonetis TD. DNA replication stress as an Achilles' heel of cancer. *Oncotarget.* 2015;1:1-2

3. Bartek J, Mistrik M, Bartkova J. Thresholds of replication stress signaling in cancer development and treatment. *Nat Struct Mol Biol.* 2012;19:5-7.

4. Jackson SP, Bartek J. The DNA-damage response in human biology and disease. *Nature.* 2009;461:1071-1078.

5. Kastan MB, Bartek J. Cell-cycle checkpoints and cancer. *Nature.* 2004;432:316-323.

6. Benada J, Macurek L. Targeting the checkpoint to kill cancer cells. *Biomolecules.* 2015;3:1912-1937.

7. Finn RS, Aleshin A, Slamon DJ. Targeting the cyclin-dependent kinases (CDK) 4/6 in estrogen receptor-positive breast cancers. *Breast Cancer Res.* 2016;18:17.

8. Hanahan D, Weinberg RA. Hallmarks of cancer: the next generation. *Cell.* 2011;144:646-674.

9. Manic G, Obrist F, Sistigu A, Vitale I. Trial Watch: Targeting ATM–CHK2 and ATR–CHK1 pathways for anticancer therapy. *Mol Cell Oncol.* 2015;2:e1012976.

10. Weber AM, Ryan AJ. ATM and ATR as therapeutic targets in cancer. *Pharmacol Ther.* 2014; 149:124-138.

11. Abraham RT. Cell cycle checkpoint signaling through the ATM and ATR kinases. *Genes Dev.* 2001;15:2177-2196.

12. Pleasance ED, Cheetham RK, Stephens PJ, et al. A comprehensive catalogue of somatic mutations from a human cancer genome. *Nature.* 2010;463:191-196.

13. Musgrove EA, Caldon CE, Barraclough J, Stone A, Sutherland RL. Cyclin D as a therapeutic target in cancer. *Nat Rev Cancer.* 2011;11:558-572.

14. Hamilton E, Infante JR. Targeting CDK4/6 in patients with cancer. *Cancer Treat Rev.* 2016;45:129-138.

15. VanArsdale T, Boshoff C, Arndt KT, Abraham RT. Molecular Pathways: Targeting the cyclin D-CDK4/6 axis for cancer treatment. *Clin Cancer Res.* 2015;21:2905-2910.

16. Yu Q, Sicinska E, Geng Y, et al. Requirement for CDK4 kinase function in breast cancer. *Cancer Cell.* 2006;9:23-32.

17. Landis MW, Pawlyk BS, Li T, Sicinski P, Hinds PW. Cyclin D1-dependent kinase activity in murine development and mammary tumorigenesis. *Cancer Cell.* 2006;9:13-22.

18. Bartkova J, Lukas J, Muller H, Lutzhoft D, Strauss M, Bartek J. Cyclin D1 protein expression and function in human breast cancer. *Int J Cancer.* 1994;57:353-361.

19. Dickson C, Fantl V, Gillett C, et al. Amplification of chromosome band 11q13 and a role for cyclin D1 in human breast cancer. *Cancer Lett.* 1995;90:43-50.

20. Yu Q, Geng Y, Sicinski P. Specific protection against breast cancers by cyclin D1 ablation. *Nature.* 2001;411:1017-1021.

21. Akervall JA, Michalides RJ, Mineta H, et al. Amplification of cyclin D1 in squamous cell carcinoma of the head and neck and the prognostic value of chromosomal abnormalities and cyclin D1 overexpression. *Cancer.* 1997;79:380-389.

22. Betticher DC, Heighway J, Hasleton PS, et al. Prognostic significance of CCND1 (cyclin D1) overexpression in primary resected non-small-cell lung cancer. *Br J Cancer.* 1996;73:294-300.

23. Bleeker FE, Lamba S, Rodolfo M, et al. Mutational profiling of cancer candidate genes in glioblastoma, melanoma and pancreatic carcinoma reveals a snapshot of their genomic landscapes. *Hum Mutat.* 2009;30:E451-459.

24. Curtin JA, Fridlyand J, Kageshita T, et al. Distinct sets of genetic alterations in melanoma. *N Engl J Med.* 2005;353:2135-2147.

25. Freedman JA, Tyler DS, Nevins JR, Augustine CK. Use of gene expression and pathway signatures to characterize the complexity of human melanoma. *Am J Pathol.* 2011;178:2513-2522.

26. Brennan CW, Verhaak RG, McKenna A, et al. The somatic genomic landscape of glioblastoma. *Cell.* 2013;155:462-477.

27. Toogood PL, Harvey PJ, Repine JT, et al. Discovery of a potent and selective inhibitor of cyclin-dependent kinase 4/6. *J Med Chem.* 2005;48:2388-2406.

28. Valkó K. Application of high-performance liquid chromatography based measurements of lipophilicity to model biological distribution. *Journal Chromatogr A.* 2004;1037:299-310.

29. Valkó K, Bevan C, Reynolds D. Chromatographic Hydrophobicity Index by Fast-Gradient RP-HPLC: A High-Throughput Alternative to log P/log D. *Anal Chem.* 1997;69:2022-2029.

30. Schaer DA, Beckmann RP, Dempsey JA, et al. The CDK4/6 inhibitor abemaciclib induces a T cell inflamed tumor microenvironment and enhances the efficacy of PD-L1 checkpoint blockade. *Cell Rep.* 2018;22:2978-2994.

31. McCain J. First-in-Class CDK4/6 inhibitor palbociclib could usher in a new wave of combination therapies for HR+, HER2− breast cancer. *PT.* 2015;8:511-520.

32. Knudsen ES, Witkiewicz AK. The strange case of CDK4/6 inhibitors: mechanisms, resistance, and combination strategies. *Trends Cancer.* 2017;3:39-55.

33. O'Leary B, Finn RS, Turner NC. Treating cancer with selective CDK4/6 inhibitors. *Nat Rev Clin Oncol.* 2016;13:417-430.

34. Pandey K, An HJ, Kim SK, et al. Molecular mechanisms of resistance to CDK4/6 inhibitors in breast cancer: A review. *Int J Cancer.* 2019;5:1179-1188.

35. Herrera-Abreu MT, Palafox M, Asghar U, et al. Early adaptation and acquired resistance to CDK4/6 inhibition in estrogen receptor-positive breast cancer. *Cancer Res.* 2016;76:2301-2313.

36. Valeur E, Bradley M. Amide bond formation: beyond the myth of coupling reagents. *Chem Soc Rev.* 2009;38:606-631.

37. Carney B, Carlucci G, Salinas B, et al. Non-invasive PET imaging of PARP1 expression in glioblastoma models. *Mol Imaging Biol.* 2016;18:386-392.

38. O'Brien N, Conklin D, Beckmann R, et al. Preclinical activity of abemaciclib alone or in combination with antimitotic and targeted therapies in breast cancer. *Mol Cancer Ther.* 2018;17:897-907.

39. Hendricks JA, Keliher EJ, Marinelli B, Reiner T, Weissleder R, Mazitschek R. In vivo PET imaging of histone deacetylases by 18F-suberoylanilide hydroxamic acid (18F-SAHA). *J Med Chem.* 2011;54:5576-5582.

FIGURES

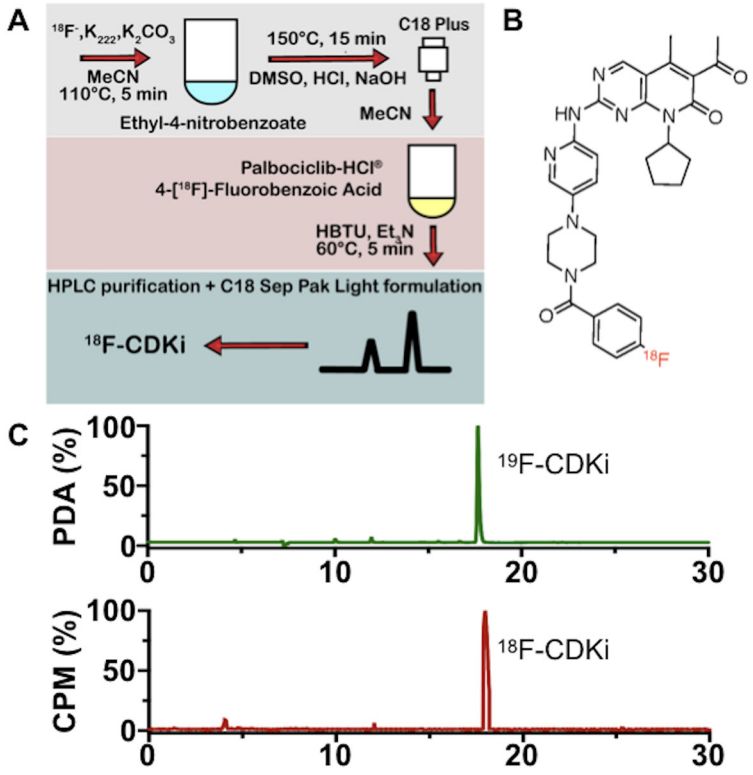

FIGURE 1: ^{18}F-CDKi. Radiochemistry and production method (A). The chromatograms represent a co-injection of ^{18}F-CDKi (B) with ^{19}F-CDKi and show the successful synthesis and purity of the PET tracer (C).

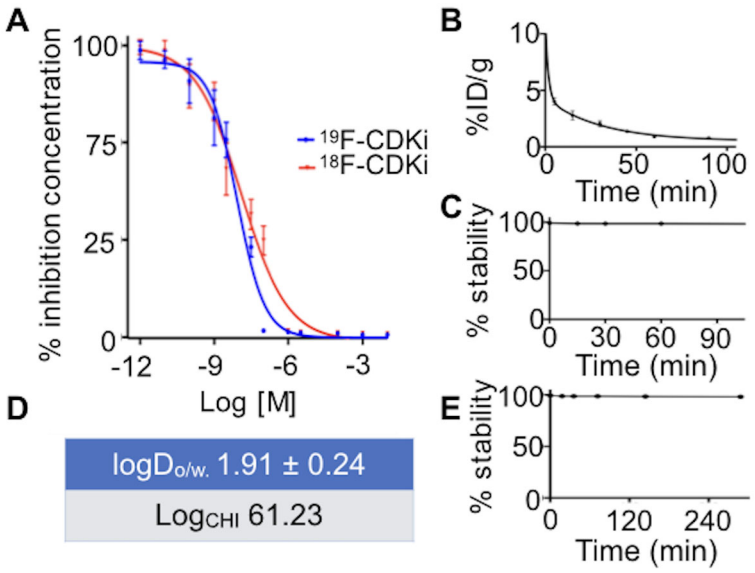

FIGURE 2: ^{18}F-CDKi/^{19}F-CDKi shows nanomolar binding affinity to CDK4/6 (A). ^{18}F-CDKi displays a 7 minutes blood half-life (B), high in vitro and in vivo stability (C and D) and lipophilic behavior (E).

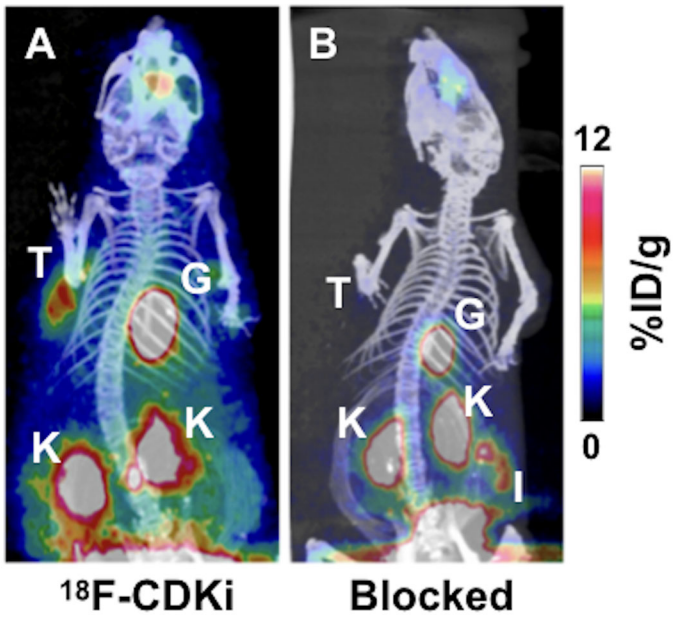

FIGURE 3: in vivo microPET/CT of MCF-7 bearing mouse models. Left panel shows a single one-bolus injection of ^{18}F-CDKi (7.4 mBq acquired at 2 h p.i.). Right panel shows a control MCF-7 mouse (pre-injected with an excess of palbociclib 30 min prior to ^{18}F-CDKi, 7.4 mBq acquired at 2 h p.i.). Active areas in scans, from top to bottom, are nasal epithelium and Harderian glands, tumor (T), gallbladder (G), kidneys (K) and intestines (I).

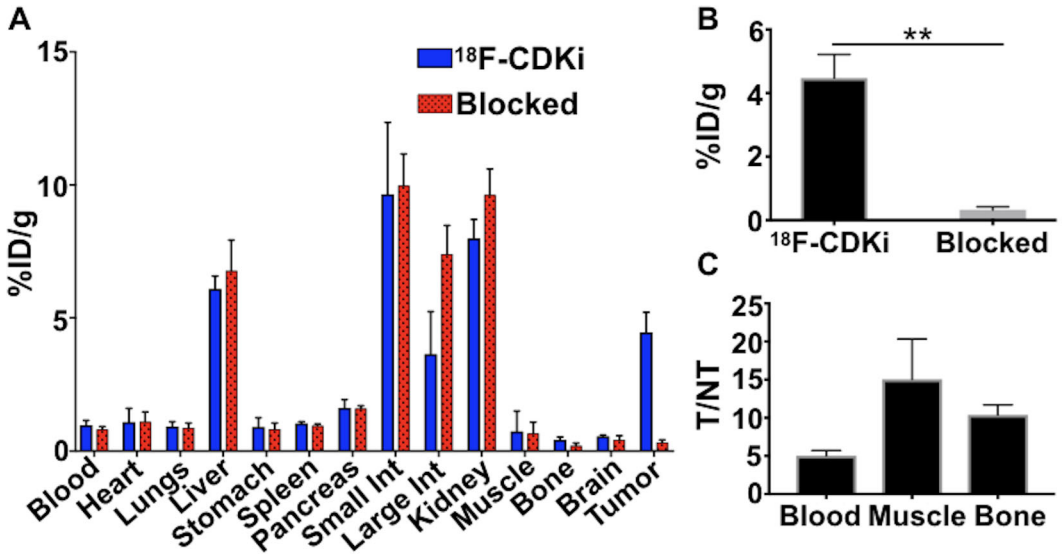

FIGURE 4: (A) ex-vivo biodistribution (2h p.i.) with a single ^{18}F-CDKi or with a pre-injection of palbociclib (blocked). (B) shows the significance in tumor %ID/g between ^{18}F-CDKi and blocked control group and (C) a representation of tumor-to-non-target blood, -muscle, or –bone ratio (n=4).

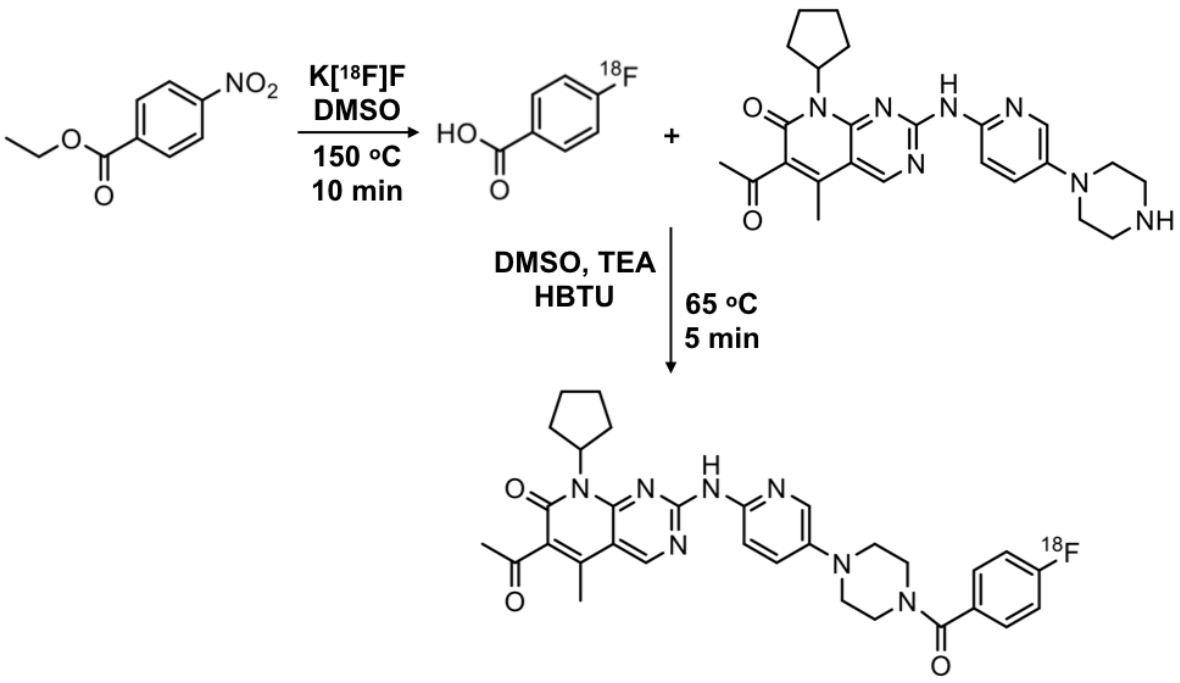

SUPPL. FIGURE 1: Synthetic radiolabeling strategy.

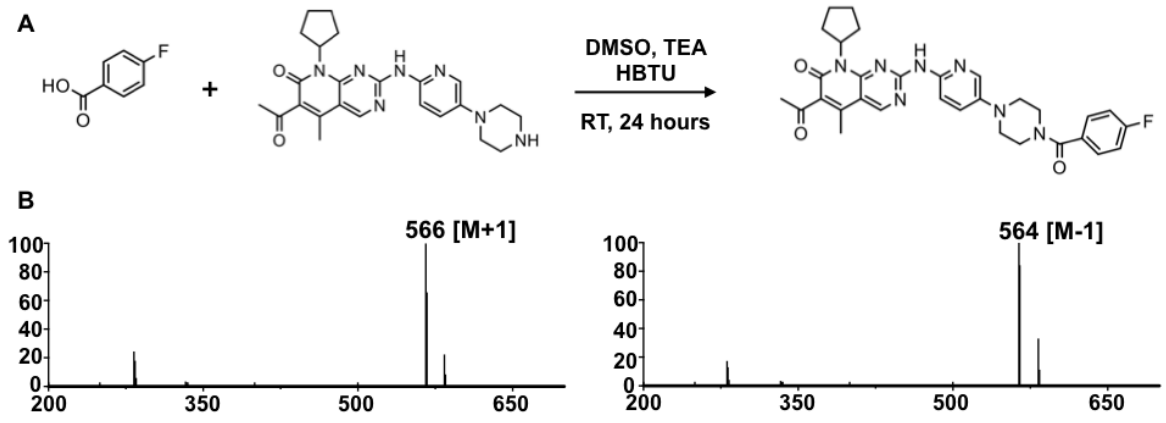

SUPPL. FIGURE 2: Synthetic radiolabeling strategy.

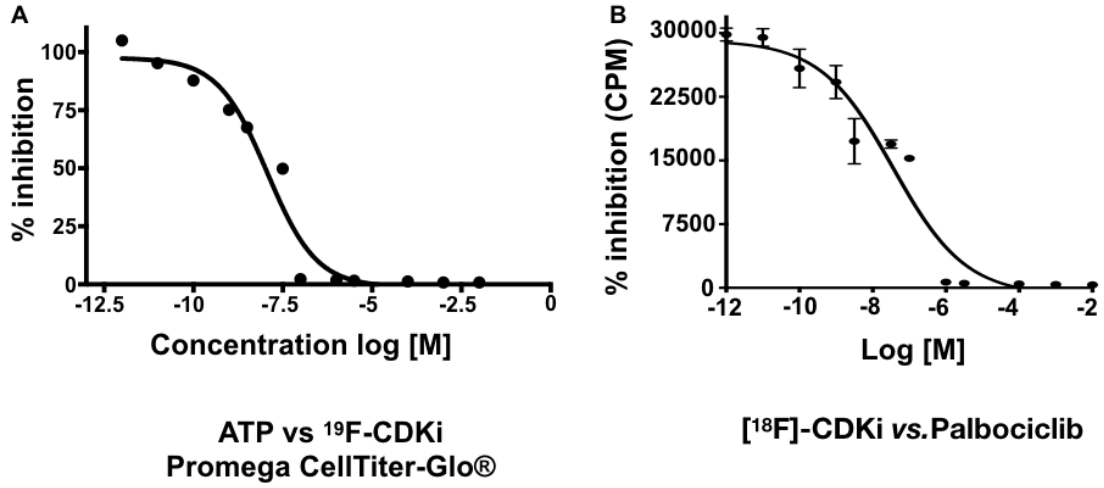

ATP vs ^{19}F-CDKi
Promega CellTiter-Glo®

[^{18}F]-CDKi *vs.* Palbociclib

SUPPL. FIGURE 3: IC50 determination

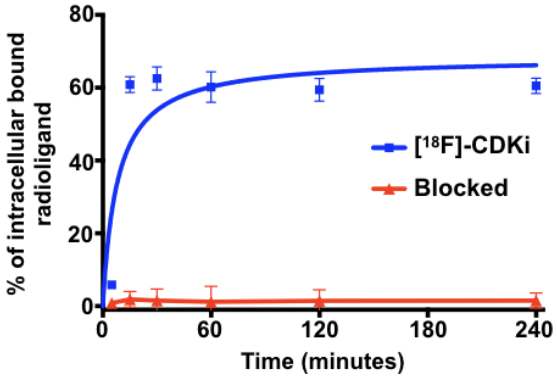

SUPPL. FIGURE 4: in vitro [^{18}F]-CDKi uptake.

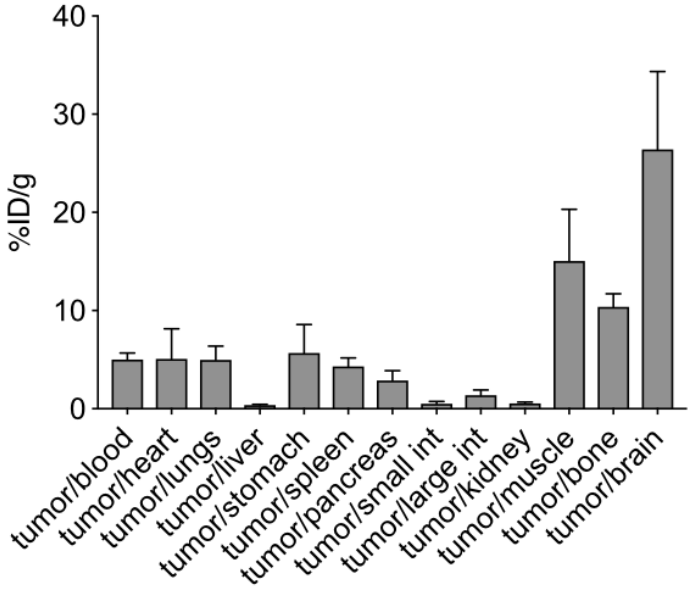

SUPPL. FIGURE 5: Tumor-to-non-target tissue ratio